Biaxial low temperature superplasticity of AA 5083 produced by accumulative roll bonding (ARB)

B.N.L McBride[1*], N. Brown[1], N. Surghani[1], V. Svaldi[1], R. Mountford[1], A.J. Clarke[1], K.D. Clarke[1]

[1]Colorado School of Mines George S Ansell Department of Metallurgical and Materials Engineering
1500 Illinois Street Golden, CO 80402
[*]corresponding author, bmcbride@mines.edu

Keywords: accumulative roll bonding, superplasticity, formability, biaxial

Abstract

Accumulative roll bonding (ARB) is a severe plastic deformation technique used to produce sub-micron grained material. Although previous studies of AA 5083 processed with ARB have demonstrated low temperature superplasticity, these studies have been limited to uniaxial tensile testing which is not representative of biaxial forming operations. Sub-micron grained samples of AA 5083 produced with ARB were subject to biaxial bulge testing using pressurized argon gas in a first-of-its-kind formability study. Thinning ratios (t_o/t_f) between 2 and 2.5 were achieved for two different deformation conditions: 225°C, 5×10^{-4} s^{-1} and 250°C, 1×10^{-3} s^{-1}. Void area fractions were less than 2% for thinning strains of 2.5, which exceeds current limits imposed on superplastic forming of conventional coarse-grained AA 5083. Average cavitation void size was smaller in sub-micron grain material than in coarse-grained material strained to similar amounts, suggesting that sub-micron grained material can be formed to higher strains prior to failure. Moreover, a 10 µm grain size is retained through deformation, leading to significant Hall-Petch strengthening in the final post-formed part. This work is an unprecedented demonstration on the exciting potential of low temperature superplasticity of AA 5083 produced by ARB under biaxial stress conditions.

Introduction

AA 5083 is a work-hardenable aluminum alloy that is commonly used in paneling applications for aircraft, automobiles and marine vessels due to its formability, weldability and corrosion resistance [1-3]. Unlike precipitation-hardenable alloys, AA 5083 can be formed directly into final part shape without need for subsequent strengthening heat treatments [2-3]. This makes the alloy desirable for high-tolerance, thin gauge sheet assemblies that may be sensitive to geometric distortion from solutionizing heat treatments. Strength is obtained through deformation and subsequent recrystallization to produce a fine-grained microstructure on the order of 10 µm; the presence of Mg solute and Al_6Mn dispersoids retain strain energy during deformation to provide the driving force for such recrystallization [1,4]. AA 5083 is known for its ability to deform superplastically by grain boundary sliding and achieve uniaxial tensile elongations in excess of 200% [1-4]. Under biaxial conditions, superplasticity can be

used to form intricate sheet components in a process known as superplasticity forming, where a pressurized gas is used to deform a sheet into the shape of an open die cavity. This process has multiple benefits over conventional forming operations, such as stamping, which include less frictional affects associated with hard tooling, smaller achievable radii of curvature in final part design, and the avoidance of spring-back [2-5]. This technology has readily been adopted by the aerospace and automotive industries for weight-savings measures [2,3]. The most notable example of this is the 2018 Bentley GT Continental, the first automobile to have 100% of its outer paneling produced with superplastic forming [6]. In this example, superplastic forming has reduced multi-part subassemblies with a single, highly-engineered part, and has helped contribute to an overall 85 kg weight reduction in the structure's body [6].

Superplastic forming has exciting potential in light-weighting automotive and aeronautical vehicles for increased fuel efficiency and reduced carbon emissions. *Conventional superplasticity* in AA 5083 occurs at temperatures above 500°C ($0.92T_m$) and strain rates on the order 1×10^{-3} s^{-1} [7-9]. This combination of high temperature and low strain rate makes the current forming process highly energy- and time-intensive; two factors which counteract the attractive reduction in carbon emissions sought after for final use applications. In the past two decades multiple studies [10-13] in severe plastic deformation (SPD) processing have shown *low temperature superplasticity* to be possible at temperatures as low as 225°C ($0.62T_m$). This reduction in temperature is possible due to the accumulation of high strains during SPD processing which lead to sub-micron grained microstructures. More recent studies have shown low temperature superplasticity to be highly dependent on the existence of non-equilibrium grain boundaries, which increase grain boundary diffusivity and therefore decrease the energy barrier for accommodating deformation mechanisms [13,14]. It has been postulated that 225°C is the lowest temperature at which sub-micron AA 5083 demonstrates appreciable superplasticity, as temperatures below this result in significant solute drag effects [13].

Accumulative roll bonding (ARB) is one of the aforementioned processing methods used to produce sub-micron grains. ARB processing is advantageous over other SPD methods such as high pressure torsion (HPT) and equal channel angular pressing (ECAP) in that bulk specimens can be produced using conventional processing equipment [13]. Additionally, the thin sheet geometry necessary for ARB processing is directly applicable to the sheet forming industry. Despite the utility of ARB as an industrially-relevant technique, a large gap remains between research-scale testing and industrial-scale production. Although numerous studies on uniaxial and biaxial superplasticity of coarse-grained material have been published [7,16-20], most studies on material produced by ARB are limited to uniaxial tensile testing [10-13]. The reason for this shortcoming is likely due to the difficulty in developing a consistent, reliable ARB process that produces samples large enough for formability testing without suffering from edge cracking [12,15]. This deficiency limits current understanding of the forming potential of

ARBed material and does not consider the anisotropic effects attributed to texture banding or elongated grain structures [21,22].

Pressurized fluid bulge testing is a laboratory scale test method used to simulate superplastic blow forming [17,18,23]. A sheet sample is clamped within a set of dies and subject to pressurized gas on one side causing the sample to deform into an open die cavity. During deformation, a strain distribution develops from the apex to the equator of the bulge with the stress state at the top of the bulge being analogous to a hoop stress [23]. The height of the bulge and thinning ratio at the apex are used to quantify the forming potential. Bulge testing is unique in that a biaxial stress is imposed without introducing frictional effects from hard tooling, such as a punch or mandrel.

Although an ASTM standard for bulge testing exists [24], it has not been readily adopted for use with ARBed material. This is because the required specimen size (100 mm diameter disc) [24] is rather large for ARB samples, which are generally on the order of 50 mm wide due to laboratory-scale rolling mill load limitations [12,15]. Moreover, this standard fails to provide specification pertaining to gas pressured that should be used during forming. Alternatively, analytical models [23] have shown to be extremely useful in calculating suitable gas pressures for bulge testing through the relationship

$$P = \frac{4s_o\sigma}{r} e^{-\dot{\varepsilon}t}\sqrt{e^{-\dot{\varepsilon}t}(1 - e^{-\dot{\varepsilon}t})} \quad (1)$$

where P is the required forming pressure, s_o is the initial sheet thickness and r is the radius of a circular die cavity. Variables σ, $\dot{\varepsilon}$ and t have their usual meaning as stress, strain rate and time expressed as von Mises equivalents; this equates uniaxial tensile stress to in-plane biaxial stress and the imposed tensile strain to thinning strain of the bulge specimen [23]. It is important to note this relationship only models deformation behavior at the apex of the bulge specimen.

In the past few decades multiple studies have been published on biaxial formability of coarse-grained superplastic materials [23,25–27], uniaxial low temperature superplasticity testing of sub-micron grained material [10-13,28] and room temperature biaxial formability of ARBed materials [29]. To date, there has not been a study on the low temperature biaxial formability of sub-micron grained material produced by accumulative roll bonding, nor has there been a comparison between uniaxial and biaxial stress states during deformation. The results presented herein are first-of-a-kind and instrumental in bridging the gap between small-scale uniaxial tension tests and industrially relevant biaxial deformation for low temperature superplasticity.

Methodology

Sheets of 1 mm thick sub-micron grained AA 5083 were produced using 5 ARB cycles having initial composition as detailed in Table 1. Sheets to be bonded were cleaned with acetone, wire-brushed, bound together

with copper wire and inserted into a constraining frame prior to rolling [12,15]. These techniques have been instrumental in mitigating edge cracking and producing samples wide enough (32 mm) for subsequent formability studies [15]. Roll bonding was conducted using unlubricated 50% reduction passes with a 133 mm two-high rolling mill operating at 37 RPM. Preheating at 250°C was conducted to reduce flow stresses and encourage bonding, but was kept to 5 min to reduce the propensity for strain recovery. The microstructure after ARB processing had a mean grain size between 250 and 500 nm and a HAGB fraction around 0.8, as previously reported [22].

Table 1 Composition of as-received AA 5083 (wt. %).

Mg	Mn	Cr	Cu	Fe	Si	Ti	Zn	Al
4.32	0.44	0.06	0.04	0.30	0.11	0.01	0.07	bal

The biaxial forming apparatus consisted of a die set with a 25.4 mm diameter cavity situated in a hydraulic press, as shown in Fig. 1. Both the dies and press platens were heated with closed-loop PID control. Square 32 x 32 x 1 mm samples were placed in the preheated die set and a preload of 18 kN was applied by the platens to prevent material draw-in during forming. Each sample was given 15 minutes to reach thermal equilibrium; this has been shown to maximize superplastic performance while minimizing grain growth of material processed with ARB [13,22]. Pressurized argon was delivered to one side of the sample by means of a compressed gas cylinder connected to a manually-regulated pressure manifold. Samples were allowed to deform freely into the open die cavity for 10, 20 and 30 minutes to represent different interrupted strain states. The back side of the sample was exposed to atmospheric pressure (i.e. no back-pressure).

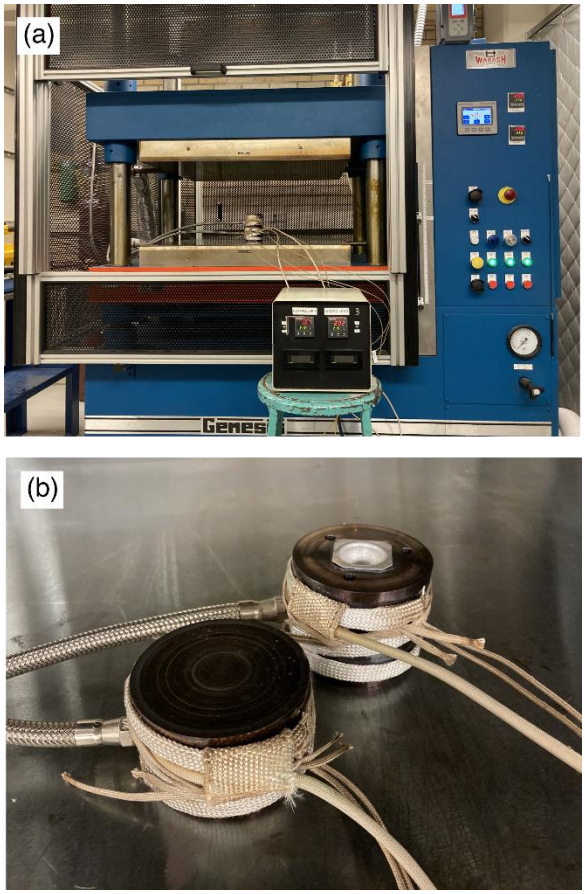

Figure 1 Bulge testing setup (a) used to evaluate superplasticity under biaxial stress conditions. A 32 x 32 mm x 1 mm sheet is centered between the dies (unstacked, (b)) and the platens are closed to provide a clampdown force while pressurized argon gas is delivered. Flexible heating tapes maintain a constant die temperature by means of a dual-zone heater controller.

Two testing conditions —225°C, 5×10^{-4} s^{-1} and 250°C, 1×10^{-3} s^{-1} — were previously identified [13] as providing optimal uniaxial low temperature superplasticity and are the focus of this study. Uniaxial flow curves of ARBed ($d\approx1$ µm) and coarse-grained material ($d\approx10$ µm) under these conditions are shown in Fig. 2. The ARBed condition exhibits superplasticity with a constantly degrading engineering stress (near constant true stress), whereas the coarse-grained sample exhibits extensive work hardening and rapid failure; superplastic deformation mechanisms are not active for coarse-grained samples under the conditions tested [13]. Forming pressures necessary to produce an equivalent biaxial stress state were calculated according to Eqn. 1 and are summarized in Table 2. Perfectly plastic behavior was assumed (i.e. no work hardening), which is a valid assumption for superplastic materials deforming by grain boundary sliding.

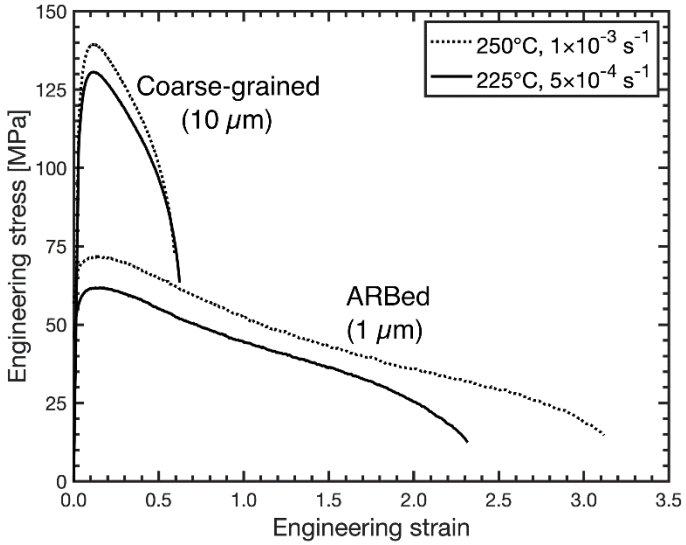

Figure 2 Uniaxial tensile flow curves of the ARBed and coarse-grained microstructures at 225°C, 5×10^{-4} s^{-1} and 250°C, 1×10^{-3} s^{-1} used to determine necessary forming pressures for biaxial bulge testing. These data were compared with other published results to determine accurate yield stresses [30].

Table 2 Summary of gas pressures necessary to replicate the uniaxial tensile stresses and strain rates for both ARBed and coarse-grained materials in a biaxial strain stress state. Equivalent stresses and strain rates are reported.

Microstructural condition	Testing condition	Equivalent flow stress	Gas pressure
5 ARB cycles	225°C, 5×10^{-4} s^{-1}	60 MPa (8.7 ksi)	6.2 MPa (0.9 ksi)
(d≈1 μm)	250°C, 1×10^{-3} s^{-1}	70 MPa (10.1 ksi)	6.9 MPa (1.0 ksi)
Coarse-grained	225°C, 5×10^{-4} s	100 MPa (14.5 ksi)	10.3 MPa (1.5 ksi)
(d≈10 μm)	250°C, 1×10^{-3} s^{-1}	75 MPa (10.9 ksi)	7.6 MPa (1.1 ksi)

Ex-situ characterization was conducted on interrupted bulge tests to calculate strain distributions and the nominal strain rate at the apex of the bulge. Cross-sectional profiles and bulge heights were obtained through 3D reconstructions of each sample using a Keyence VHX5000 microscope with 100 μm increments in focal plane height. Thinning strains were measured by optical image analysis after sectioning samples in quarters along the sheet longitudinal and transverse planes. Roughly 1.5 mm of material was lost to kerf during sectioning, making precise strain measurement at the true apex difficult. In additional to quantitative analysis, circle grids were electrolytically etched onto samples prior to deformation to qualitatively observe strain gradients.

Microstructural damage, namely cavitation voids, during biaxial bulge testing was characterized using an image analysis routine on backscatter electron (BSE) micrographs of sample cross-sections. Channeling contrast, along with manipulation of brightness and contrast, was employed to make cavitation voids appear black (no signal,

8-bit value of 0), and Fe- and Mn-containing precipitates to appear white (maximum signal, 8-bit value of 255); all other features of the matrix and precipitates have an intermediate grayscale value. Cross-sections were prepared using traditional metallographic techniques of successive grinding and polishing. A contrast threshold was applied to BSE micrographs to delineate voids from the surrounding microstructure. ImageJ's *Analyze Particles* routine was used to measure the size and shape of voids. Only voids with a minimum of four neighboring pixels were counted; a resolution of 0.2 μm/pixel was used throughout the study.

Results

There is a noticeable difference in deformation behavior between the ARBed and coarse-grained samples, as shown in Fig. 3. The ARBed samples exhibited appreciable stains after each time increment, achieving bulge heights as high as 14.0 mm for the 250°C, 5×10^{-4} s^{-1} condition. The coarse-grained samples, on the other hand, achieved significantly lower bulge heights regardless of the testing parameters used; heights around 5 mm were achieved after the first 10 minutes, but only increased to about 6 - 7 mm after the entire 30 minutes. The difference in deformation behavior between the ARBed and coarse-grained material is not surprising given the perfectly-plastic deformation assumption. The ARBed microstructure deforms by grain boundary sliding at these temperatures with near-constant flow stress [13] whereas the coarse-grained samples are deform with significant work hardening, as illustrated in Fig. 2. As a result, continued deformation in the coarse-grained samples is abruptly ceased. Due its inferior deformation performance at such low temperatures, the coarse-grained material will not be investigated to the same extent as the ARBed material for the remainder of this work.

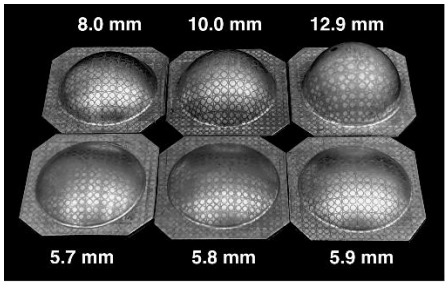

(a) 225°C, 5×10^{-4} s^{-1}

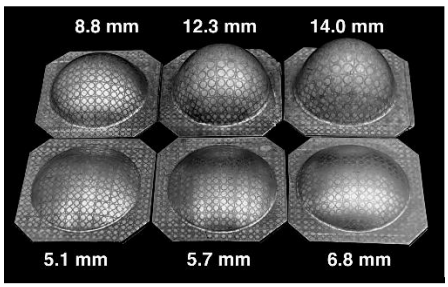

(b) 250°C, 1×10^{-3} s^{-1}

Figure 3 Samples after 10, 20 and 30 minutes (left to right) interrupted bulge testing with measured bulge height. Samples in the foreground are coarse-grained AA 5083 (10 μm); samples in the background are AA 5083 processed with 5 ARB cycles (1 um).Two testing conditions were used: (a) 225°C, 5×10^{-4} s^{-1} and (b) 250°C, 1×10^{-3} s^{-1}. Sample dimensions before testing were 32 x 32 x 1 mm.

Thinning strains at the apex of each ARBed sample were measured and compared to deformation duration to calculate the actual strain rate, summarized in Fig. 4. Samples tested at a nominal rate of 5×10^{-4} s^{-1} (225°C) deformed at strain rates between 4×10^{-4} and 6×10^{-4} s^{-1}, which represents only minimal error. The same cannot be said for samples tested at 1×10^{-3} s^{-1} (250°C), which exhibited actual strain rates between 6×10^{-4} and 8×10^{-4} s^{-1}; an absolute error on the scale of half an order of magnitude. This discrepancy between the anticipated and exhibited strain rates may be due to the greater extent of partial recrystallization that occurs during soaking at 250°C [22], which would change the flow stress necessary for steady-state deformation. Nevertheless, both conditions exhibited relatively stable strain rates through deformation, validating the assumption of constant flow stress for the ARBed condition and corroborating Eqn. 1 as a valid predictor of forming gas pressure.

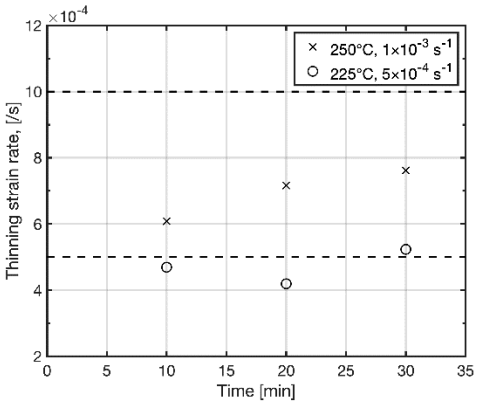

Figure 4 Measured thinning strain rates at the apex of samples tested at 225°C, 5×10^{-4} s^{-1} and 250°C, 1×10^{-3} s^{-1} for 10, 20 and 30 minutes. Observed strain rates were within half an order of magnitude of nominal values.

Cross-section profiles parallel to the original sheet rolling and transverse directions of ARBed samples are shown in Fig. 5. Bulge testing begins with a round cap evolving into a hemisphere at a height equal to half the die cavity radius: 12.7 mm. After this point, the near-vertical portion of the sample at the base bulge contacts the side walls of the die cavity and is subsequently constrained by frictional forces. Further deformation localizes toward the apex of the dome. Post-hemispherical deformation is only observed in the 250°C, 1×10^{-3} s^{-1} condition and occurs between the 20 and 30 minute mark. Regardless of the condition or strain amount, anisotropy in thinning is imperceptible at the measurement scale used.

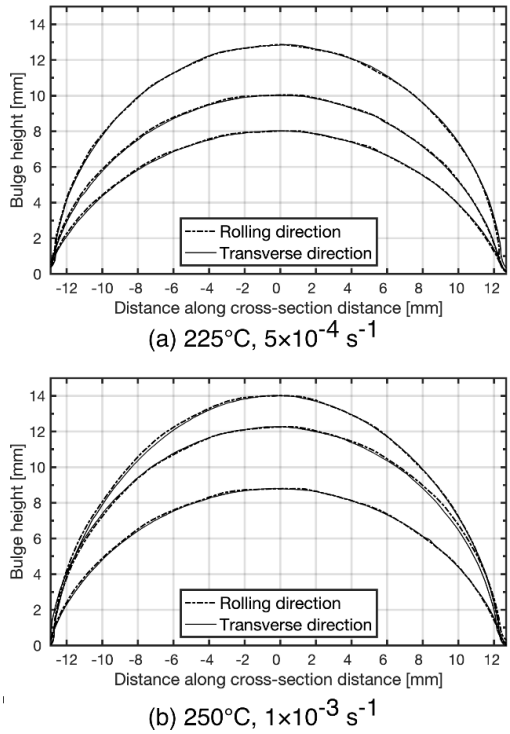

Figure 5 Bulge height cross-section profiles measured with a Keyence VHX5000 using 100 μm increments in focal plane height for the (a) 225°C, 5×10^{-4} s^{-1} and (b) 250°C, 1×10^{-3} s^{-1} conditions.

Thinning strains are a better measurement of anisotropy and are commonly used characterize formability. In superplastic sheet forming, thinning strains are commonly reported as thinning ratios (t_o/t_f), where t_o and t_f are the initial and final thicknesses, respectively. Fig. 6 shows how the thinning ratio varies along the cross-section profiles of ARBed samples tested under both conditions; the thinning ratio is 1 at the equator and increases toward the apex. The sample tested at 250°C, 1×10^{-3} s^{-1} for 30 minutes shows a more drastic increase in thinning ratio near the apex due to strain localization. This is likely due to frictional effects imposed by the side walls of the cavity, or may be due to tensile instability preceding material failure. Samples strained to failure ruptured shortly after the 30 minute mark suggesting the latter to be more probable.

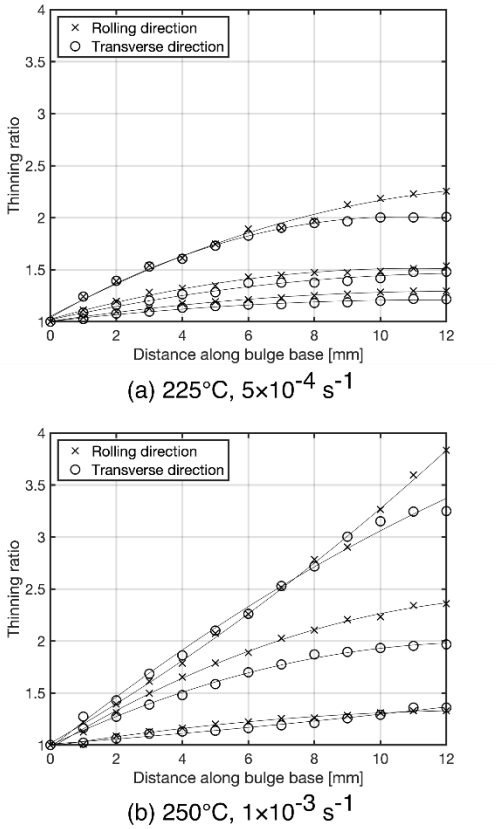

Figure 6 Thinning ratios (t_o/t_f) measured from the equator to the apex along the bulge base for the (a) 225°C, 5×10^{-4} s^{-1} and (b) 250°C, 1×10^{-3} s^{-1} conditions. Localized thinning is apparent in the 250°C, 1×10^{-3} s^{-1} condition by the inflection in the 30 min data points near the apex of the bulge.

Discussion

Thinning ratios provide critical information about the forming potential of superplastic material. Thinning ratios prior to failure were between 2 and 2.5 for both conditions, with bulge heights reaching roughly 100% of the cavity radius (i.e. a hemisphere). For comparison, industrial superplastic forming operations are typically limited to thinning ratios around 2 to ensure adequate part strength [2-4]; thus, the superplastic formability demonstrated by sub-grained material is on-par with industrial expectations.

Achieving higher thinning ratios is limited by cavitation voids that form as an undesirable consequence of grain boundary sliding [3]. Such voids occur when the imposed strain rate cannot be satisfied by the accommodating deformation rates for grain boundary sliding [4]. These voids, shown in Fig. 7, grow and coalesce with increased strain in a fashion analogous to external necking in tension, ultimately leading to failure due to a reduce load-carrying capacity [31]. Voids, with mean radius around 1.5 μm, preferentially nucleate at previous bonding interfaces and exhibit faster growth rates in the top half of the sample thickness; this is unsurprising, as the geometry of the hemisphere would require larger in-plane strains at the top. It is common practice to restrict void area fractions in formed parts to 2% or lower to retain mechanical strength, which leads to the thinning ratio limit of 2 [2-

3]; thinning ratios above 2.5 have exhibited void fractions that exceed 2-5% in coarse-grained AA 5083 [16-18]. On the contrary, ARBed samples demonstrated thinning ratios near 3 for void area fractions less than 2%. Continued deformation to higher strains leads to increased void fraction, consistent with the localized thinning reported in Fig. 6.

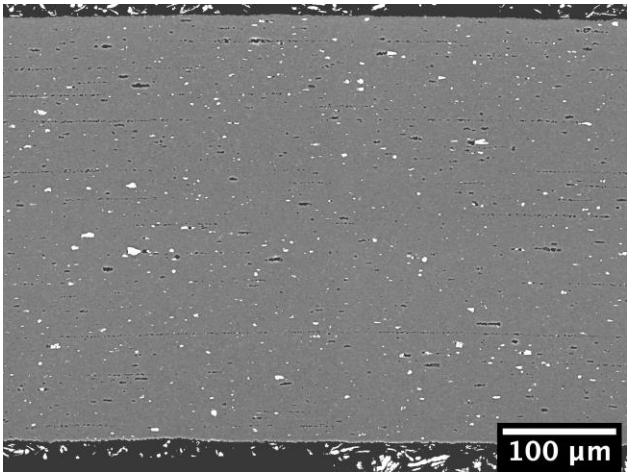

Figure 7 Cross-section near the apex of a bulge specimen tested at 250°C, 1×10^{-3} s^{-1} for 20 minutes. The plane shown corresponds to the original longitudinal plane of the ARBed samples. The thinning ratio is approximately 2.6.

High thinning ratios are limited not only by the area fraction of voids, but also their size and distribution. Fig. 8 summarizes void area fraction and size for both testing conditions. Voids remains under 2 µm for thinning ratios up to 3, after which void growth accelerates rapidly in the same manner as area fraction. These voids are notably smaller than in coarse-grained material [16-18] which are on the scale of tens of micrometers, validating the hypothesis that voids are typically comparable to the grain size of the material [4]. On the other hand, the reported void area fraction and size arising from biaxial testing of ARBed samples is notably larger than those from uniaxial tensile testing, despite similar equivalent strain levels [13]. It appears biaxial deformation is more damaging in terms of void formation [4] but is also less susceptible to strain localization.

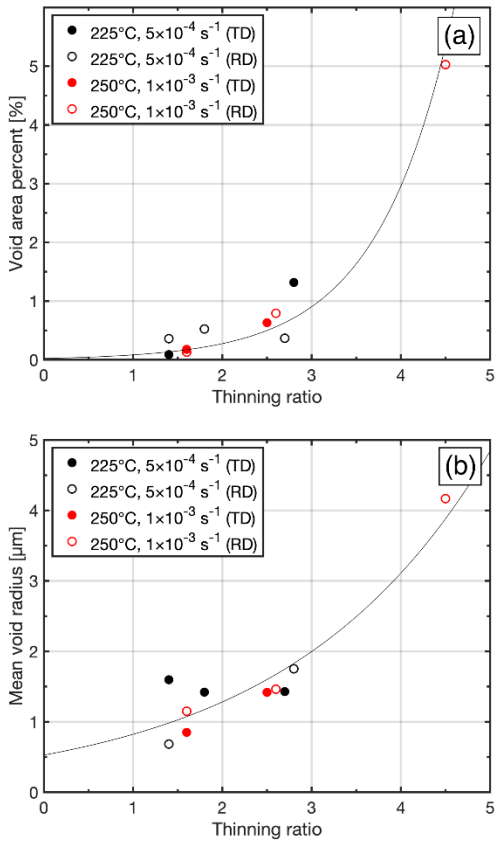

Figure 8 Void fraction (a) and mean void radius (b) measured at the apex of bulges strained to different amounts. High void fractions and radii in the 250°C, 1×10^{-3} s^{-1}, 30 min condition are indicative of localized thinning.

The pre-formed strength (≈300 MPa) of conventional coarse-grained superplastic AA 5083 (10 µm, 500°C, 1×10^{-3} s^{-1}) can be retained if void area fractions are kept below 2% [32]. Applying the same criteria to sub-micron grained material produced by ARBed, which exhibits extensive Hall-Petch strengthening, suggests post-formed strengths between 400 to 500 MPa may be realized in final sheet components if the grain size can be retained [33,34]. The microstructure of the sample deformed at 250°C, 1×10^{-3} s^{-1} is shown through back-scatter electron micrographs in Fig. 9. Post-formed grain size at the sample apex is roughly 1 µm, in agreement with previous work by the authors examining microstructural evolution during both static annealing [13] and uniaxial superplasticity [22]. The impact of submicron grain size retention during forming is twofold: sheet components can be formed with higher strains (e.g. thinner) while still meeting current strength performance, and less components may be required in an assembly to meet desire criteria due to the increased strength provided.

Fig. 9 shows that voids appear to nucleate at secondary phases [4], suggesting precise control of precipitation prior to superplastic forming may be advantageous in reducing overall cavitation damage. Comparing Fig. 7 and Fig. 9, however, it is evident that void formation is more closely related to ARB bonding interfaces than precipitation distribution through the microstructure. Although void nucleation at precipitates is undoubtedly a concern during superplasticity in general [4], it is not the focus of this current study and will not be discussed in more detail.

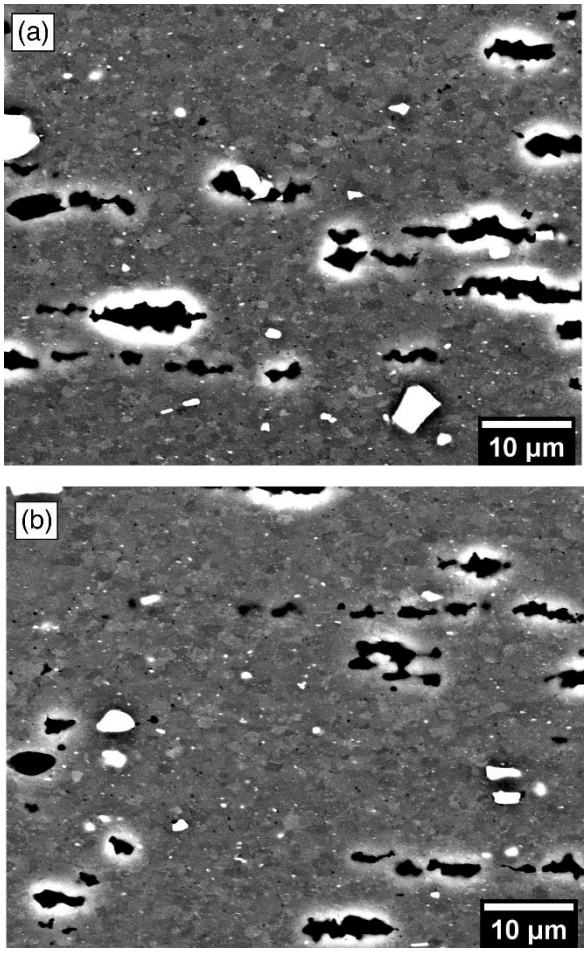

Figure 9 Channeling contrast backscatter electron micrographs showing relative grain and void size taken near the (a) top and (b) bottom of apex of a sample tested in the 250°C, 1×10^{-3} s^{-1}, 20 min condition. The thinning ratio is approximately 2.6. Regions appearing black are cavitation voids. White regions surrounding voids are an artefact of the incident electron beam interacting with the thin volume of the void edge.

Comparing the bulge heights in Fig. 5, the thinning ratios in Fig. 6 and the void character in Fig. 8 it remains unclear if anisotropy exists between the transverse and rolling directions. Slight differences between parameters may be due to error associated with sectioning samples on cross-sectional planes which precisely intersect the apex of the bulge. Furthermore both continuous static and continuous dynamic recrystallization [13,22] lead to a more equiaxed microstructure prior to high strain deformation which may remove significant sources of anisotropy. The nature of grain boundary sliding may also lend itself to reduce anisotropy; sliding commences along favorably oriented grains until an obstacle is encountered. The apex of the specimen experiences radial tensile stresses which could activate grain boundary sliding along multiple boundary orientations simultaneously, thus avoiding a directional dependence of deformation. Anisotropy cannot be discounted without further evaluation, but the results presented suggest anisotropy effects, if any, are minor.

It is worth mentioning the experimental design in this study presents only a subset of all possible parameters that may have an influence on formability. Lubrication along the cavity radius was not used which may have led to an earlier onset of localized thinning. The geometry chosen was necessarily small due to the limitations of ARB processing, which meant relatively small aspect ratios (cavity diameter to sheet thickness) were used compared to other studies (25.4 compared to 50-100 [17,18]). The final utility of superplastic formed sub-micron grained material will be limited the initial sheet thickness, which is currently on the order of 1-2 mm. Lastly, it is worth noting back pressure was not used for testing described here, although it has been shown to drastically reduce cavitation voids from 2.5 % to 0.3 % for thinning ratios around 2 [35]. Back pressure may be another avenue to further increase the formability of sub-micron grained material.

Conclusions

The results presented here are a novel demonstration of the advantages of using severe plastic deformation to engineer microstructures with increased forming potential. Small-scale bulge testing demonstrated high strain ratios between 2 and 2.5 were achieved with void area fractions below 2% —what is typically considered the industrial standard. Most impressively, forming to these high strains was possible at temperatures of 225°C ($0.59T_m$) and 250°C ($0.62T_m$) for strain rates of 5×10^{-4} s^{-1} and 1×10^{-3} s^{-1}, respectively. These temperatures are significantly lower than what is conducted industrially ($0.92T_m$) while still maintaining similar strain rates, indicating potential cost-saving opportunities.

The two testing conditions described herein were previously identified as optimal for low temperature uniaxial superplasticity despite have different strain rate sensitivities: $m = 0.45$ for 250°C, 1×10^{-3} s^{-1} and $m = 0.40$ for 225°C, 5×10^{-4} s^{-1} [13]. A more extensive evaluation would be needed to compare the strain localization behavior as a function of biaxial forming parameters to ascertain if one condition is more suited for formability than the other. From the results demonstrated, both conditions demonstrate comparable biaxial low temperature superplastic formability.

Bulge testing has been shown to be a vital forming technique to evaluate industrially-relevant low temperature superplasticity. More so, the analytical model for forming gas pressure showed excellent agreement between uniaxial and biaxial testing scenarios even when extended to lower temperatures. The results presented complement uniaxial testing results [13] and emphasize the importance of strain state in quantifying formability for industrial applications. Although the rate of void growth is higher under biaxial stress conditions, strain localization does not

appear to be as catastrophic. Moreover, material produced with ARB does not appear to have significant anisotropy when comparing the rolling and transverse directions.

Superplastic forming of sub-micron grained AA 5083 may provide additional benefits over conventionally processed material, including a smaller void area fraction at higher strains and a greater final part strength attributed to sub-micron grain size retention. These factors combined amplify the already promising cost-benefit of temperature reduction in superplastic sheet forming. This first-of-its kind study is fundamental in strengthening the connection between laboratory- and industrial-scale low temperature superplasticity, and establishes a precursor to future developments in sheet formability.

Acknowledgments

The work herein is a part of the Center for Advanced Non-Ferrous Structural Alloys (CANFSA), a National Science Foundation (NSF) Industry-University Cooperative Research Center (IUCRC). Additional acknowledgments are attributed to J. Carpenter of Los Alamos National Laboratory (LANL) and M. Ciemiorek-Bartowska of Politechnika Warszawska for their support in ARB processing and biaxial formability.

[1] G. Totten and D. MacKenzie, *Handbook of Aluminum: Vol. 1: Physical Metallurgy and Processes*, Taylor & Francis, 2003.
[2] A. J. Barnes, Superplastic Forming 40 Years and Still Growing, J. Mater. Eng. Perform., vol. 16, no. 4, pp. 440–454, 2007.
[3] A. J. Barnes, H. Raman, A. Lower, and D. Edwards, Recent Application of Superformed 5083 Aluminum Alloy in the Aerospace Industry, Mater. Sci. Forum, vol. 735, pp. 361–371, 2013.
[4] J. Pilling and N. Ridley, *Superplasticity in crystalline solids*, Institute of Metals London, 1989.
[5] R. Koganti and J. Weishaar, Aluminum Vehicle Body Construction and Enabling Manufacturing Technologies, SAE Int. J. Mater. Manuf., vol. 1, no. 1, pp. 491-502, 2009.
[6] Hydro introduces new alloys for superplastic forming of complex automotive components. Light Metal Age, pages 28-31, December 2018.
[7] R. Verma, A.K. Ghosh, S. Kim and C. Kim, Grain refinement and superplasticity in 5083 Al, Mater. Sci. Eng. A, 1995, 191, p 143–150.
[8] R.M. Cleveland, A.K. Ghosh and J.R. Bradley, Comparison of superplastic behavior in two 5083 aluminum alloys, Mater. Sci. Eng. A, 2004, 351(1-2), p 228–236.
[9] H. Jin, Optimization of Aluminum Alloy AA5083 for Superplastic and Quick Plastic Forming, Metal. Mater. Trans., A., 2019, 50(8) p 3868-3890.
[10] N. Tsuji, K. Shiotsuki and Y. Saito, Superplasticity of ultra-fine grained Al-Mg alloy produced by accumulative roll bonding. Mater. Trans., JIM, 1999, 40(8), p 765–771.
[11] I.C. Hsiao and J.C. Huang, Deformation Mechanisms during low- and high- temperature superplasticity in 5083 Al-Mg alloy, Metall. Mater. Trans., A, 2002, 33A, p 1373-1384.
[12] Y. Saito, H. Utsunomiya, N. Tsuji, and T. Sakai, Novel ultra-high straining process for bulk materials - development of the accumulative roll bonding (ARB) Process, Acta Mater., 1999, 47(2), p 579–583.
[13] B.N.L McBride, A.J. Clarke and K.D. Clarke, The limits of low temperature superplasticity in AA 5083 produced by accumulative roll bonding (ARB), Mater. Met. Trans., A, March 2020, in review.
[14] X. Sauvage, G. Wilde, S.V. Divinski, Z. Horita and R.Z. Valiev, Grain boundaries in ultrafine grained materials processed by severe plastic deformation and related phenomena, Mater. Sci. Eng. A, 2012, 540, p 1–12.
[15] B.N.L McBride, K.D Clarke, A.J. Clarke, Mitigation of edge cracking during accumulative roll bonding (ARB) of aluminum strips, J. Manuf. Process., 2020, 55, p 236-239.

[16] R. Verma, PA. Friedman, A.K. Ghosh, C. Kim, and S. Kim, Superplastic forming characteristics of fine-grained 5083 aluminum, J. Mater. Eng. Perform., 1995, 4, p. 543–550.
[17] Y. Luo, C. Miller, G. Luckey, P. Friedman, and Y. Peng, On practical forming limits in superplastic forming of aluminum sheet, J. Mater. Eng. Perform., 2007, 16, p. 274-283.
[18] P.H. Sun, H.Y. Wu, W.S. Lee, S.H. Shis, J.Y. Perng, and S. Lee, Cavitation behavior in superplastic 5083 Al alloy during multiaxial gas blow forming with lubrication, Int. J. Mach. Tools Manuf., 2009, 49, p.13–19.
[19] O. Majidi, M. Jahazi, N. Bombardier, Prediction of material behavior during biaxial stretching of superplastic 5083 aluminum alloy, Int. J. Adv. Manuf. Technol, 2019, 102, p. 2357–2366.
[20] M. Balasubramanian, P. Ganesh, K. Ramanathan, V.S.S. Kumar, Superplastic Forming of a three-stage hemispherical 5083 aluminium Profile, J. Mech. Eng., 2015, 61(6) p. 365-373.
[21] M. Reza-Toroghinejad, F. Ashrafizadeh, R. Jamaati, M. Hoseini, and J.A. Szpunar, Textural evolution of nanostructured AA5083 produced by ARB, Mater. Sci. Eng. A, 2012, 556, p. 351-357.
[22] B.N.L. McBride, M.D. Sanders, A.J. Clarke, K.D. Clarke, Retention of sub-micron grains through continuous recrystallization of AA 5083 produced by accumulative roll bonding (ABR), Metall. Mater. Trans A, submitted February 2022.
[23] A. Dutta and A.K. Mukherjee, Superplastic forming: an analytical approach. Mater. Sci. Eng. A, 1992, 7, p. 9-13.
[24] ASTM-E2712: Standard test methods for bulge-forming superplastic metallic sheet, ASTM International, West Conshohocken, PA (2015).
[25] R. Kaibyshev, I. Kazakulov, D. Gromov, D.R. Lesuer, and T.G. Nieh, Superplastic blow forming of 2219 aluminum alloy, 2004, Mater. Sci. Forum, 447-448, p. 265-270.
[26] M.E. Hosseini, S.J. Hosseinipour, and M.B. Jooybari, Analysis of void growth during superplastic deformation of commercial Al5083 alloy, Iran. J. Sci. Technol., Trans. Mech. Eng., 2018, 42, p. 41–49.
[27] H.Y. Wu, J.Y. Perng, S.H Shis, C.H. Chiu, S. Lee, and J.Y. Wang, Cavitation characteristics of a superplastic 5083 Al alloy during gas blow forming, J. Mater. Sci., 2006, 41, p. 7446–7453.
[28] Hsiao, I.C., Huang, J.C.: Development of low temperature superplasticity in commercial 5083 Al-Mg alloys. Scr. Mater., 1999, 40(6), p. 697–703.
[29] I. Topic, H.W. Höppel, D. Staud, M. Merklein, M. Geiger and M. Göken, Formability of accumulative roll bonded aluminum AA1050 and AA6016 investigated using bulge tests, 2008, Adv. Eng. Mater., 12, p. 1101–1109.
[30] P.T. Summers, Y. Chen, C.M. Rippe, B. Allen, A.P. Mouritz, S.W. Case, and B.Y. Lattimer, Overview of aluminum alloy mechanical properties during and after fires. Fire Sci. Rev., 2015, 4.
[31] S. Sagat, D.M.R. Taplin, Fracture of a superplastic ternary brass, Acta Metall., 1976, 24, p. 307-315.
[32] B. Gershon, I. Eldror, I.Arbel, and J. Milo, Problems encountered in superplastic forming of Al 5083 parts, Mater. Sci. Forum, 2004, 447-448, p. 259-264.
[33] M. Reza-Toroghinejad, F. Ashrafizadeh and R. Jamaati, On the use of accumulative roll bonding process to develop nanostructured aluminum alloy 5083. Mater. Sci. Eng. A, 2013, 561, p. 145–151.
[34] Y.B Lee, D.H. Shin, D.H., W.J. Nam, Annealing behavior of 5083 Al alloy deformed at cryogenic temperature, J. Mater. Sci., 2005, 40, p. 797–799.
[35] A.F Carunchio, D.A Pereira, M.H.F. Batalha, H.B Resende, A.S. Antunes, The effectiveness of back pressure in superplastic blow forming of aluminum alloy AA 5083 performed at very favorable conditions for cavitation growth, Mater. Res., 2018, 21 (5).